

# Characterization of Structure in Biogenic Amorphous Calcium Carbonate: Pair Distribution Function and Nuclear Magnetic Resonance Studies of Lobster Gastrolith

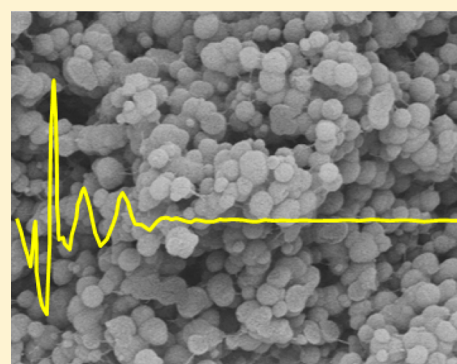
Richard J. Reeder,<sup>\*,†</sup> Yuanzhi Tang,<sup>†,§</sup> Millicent P. Schmidt,<sup>†</sup> Laura M. Kubista,<sup>†</sup> Diane F. Cowan,<sup>‡</sup> and Brian L. Phillips<sup>†</sup>

<sup>†</sup>Department of Geosciences, Stony Brook University, Stony Brook, New York 11794-2100, United States

<sup>‡</sup>The Lobster Conservancy, Friendship, Maine 04547, United States

## S Supporting Information

**ABSTRACT:** Total X-ray scattering and pair distribution function analysis are combined with nuclear magnetic resonance spectroscopy to identify key differences in structural properties between biogenic and synthetic samples of amorphous calcium carbonate (ACC). Biogenic samples studied are gastroliths taken from the American lobster and are composed of hydrated ACC containing minor impurities. X-ray pair distribution functions reveal that the short- and medium-range structure found in synthetic ACC also occurs in gastrolith ACC, notably with atomic pair correlations extending up to  $\sim 10$  Å. The  $^{13}\text{C}$  NMR spectra of gastrolith ACC show a distribution of carbonate environments as seen in synthetic hydrated ACC. However,  $^1\text{H}$  NMR spectroscopy reveals that a mobile  $\text{H}_2\text{O}$  component and hydroxyl groups found in synthetic hydrated ACC are absent in the gastrolith ACC. This difference may arise from differences in local conditions of ACC formation. The  $^{31}\text{P}$  NMR results indicate that inorganic phosphate is the principal form of the minor phosphorus. Gastrolith that was allowed to age shows the presence of calcite and vaterite, as well as residual ACC.  $^{31}\text{P}$  NMR also reveals trace amounts of monetite ( $\text{CaHPO}_4$ ) in aged samples, raising the possibility that fresh gastrolith ACC may contain a minor component of amorphous calcium phosphate. The findings suggest that important differences in the hydrous components between synthetic and biogenic hydrated ACC influence stability of the amorphous phase and its transformation to crystalline forms, thereby extending the foundation for advanced materials applications in engineered systems.



## 1. INTRODUCTION

Amorphous calcium carbonate (ACC) is known to serve multiple functions during biomineralization processes: as a transient precursor to crystalline  $\text{CaCO}_3$ ,<sup>1,2</sup> as structural components of functional hard parts,<sup>3</sup> and as temporary storage of calcium.<sup>1,4</sup> The factors controlling the behavior of ACC, including its temporary stabilization and its transformation to crystalline phases, are critical for understanding biomineralization processes. Additives such as inorganic ions (e.g.,  $\text{Mg}^{2+}$  and  $\text{PO}_4^{3-}$ ) and organic macromolecules have been identified as likely agents providing temporary stabilization<sup>5–11</sup> and may also influence subsequent transformation and polymorph selection.<sup>6</sup> Yet, the specific interactions that inhibit crystallization of ACC over a time scale necessary for its utilization, and that may also direct its subsequent crystallization, remain largely unknown. These same questions have challenged materials scientists, who have looked to biomineralization processes as models for biomimetic synthesis for advanced materials applications.<sup>12,13</sup> ACC is also thought to play a role in formation of inorganic calcium carbonates and hence may be relevant to important engineered systems, including carbon dioxide sequestration and scale formation.

One of the main limitations in understanding properties and behavior of ACC is a lack of knowledge of its structure. Different stabilities and transformation behaviors reported among ACC varieties are likely dependent on structural variations related to their mechanism of formation. Owing to the noncrystalline character of ACC, studies of its structure have mainly relied on local structure techniques. Among these, X-ray absorption spectroscopy has been most widely used. However, these studies have provided little information beyond average first-shell coordination around Ca atoms. Infrared spectroscopy has also revealed differences in vibrational bands, distinguishing ACC from crystalline  $\text{CaCO}_3$  forms.<sup>1,3,14</sup>

Recently, high-energy X-ray total scattering studies of synthetic ACC have yielded atomic pair distribution functions (PDFs), showing structural order (i.e., pair correlations) extending up to 10 or more angstroms.<sup>15</sup> In comparison to Bragg diffraction, which provides information about the average long-range order in crystalline solids, total scattering also

**Received:** November 12, 2012

**Revised:** March 19, 2013

**Published:** April 1, 2013

includes the contribution from diffuse scattering, which contains information about short- and medium-range order and is more relevant for noncrystalline materials. This total scattering study of ACC established the existence of medium-range order and provided the basis for the first structure model for hydrated ACC. The model, derived from reverse Monte Carlo (RMC) refinement of the total X-ray scattering data, shows a distribution of Ca coordination environments, encompassing the various linkages that distinguish the crystalline  $\text{CaCO}_3$  forms.<sup>16</sup> An unexpected feature of the structure model is the presence of a nanoporous network supported within a Ca-rich framework. If present, such a network could provide potential sites for additives and could also play a role during crystallization. In addition to  $\text{Ca}^{2+}$  and carbonate ions, synthetic ACC also contains approximately one mole of  $\text{H}_2\text{O}$  per mole  $\text{CaCO}_3$ . NMR spectroscopy shows that most of the H occurs in  $\text{H}_2\text{O}$  molecules with only a minor amount of H in the form of hydroxyl ions. The water molecules appear to occur as two populations, one rigid, presumably bound to Ca atoms, and the other more mobile, although less so than expected for a fluid. These recent advances in understanding of structure and dynamics have thus far been limited to laboratory-synthesized ACC.

In the present study, we utilize synchrotron X-ray total scattering to demonstrate that ACC present in the gastroliths of the American lobster, *Homarus americanus*, exhibits medium-range structural order similar to that observed in synthetic ACC. We also use NMR spectroscopy to determine the distribution of H environments, finding that they differ from those observed in synthetic, hydrated ACC. In lobster and crayfish, gastroliths are thought to serve as temporary storage of calcium during the molting process.<sup>17</sup> Gastroliths form during the premolt stage, associated with demineralization of the exoskeleton (cuticle). The gastroliths are subsequently resorbed to assist in calcification of the new exoskeleton.<sup>18</sup> Analyses of gastroliths in crayfish have shown the mineral component to be ACC,<sup>19</sup> and characterization of calcium storage structures in other crustaceans has shown them more specifically to be hydrated ACC.<sup>4,7</sup> Other components found within gastroliths include a chitin-based scaffold on which the ACC nanoparticles are supported, organic macromolecules (proteins), smaller metabolites (including citrate and organophosphates), and inorganic ions such as orthophosphate and  $\text{Mg}^{2+}$ .<sup>8,10,19,20</sup> Using NMR methods, Akiva-Tal and co-workers showed that at least some of the smaller organic molecules and orthophosphate occur dispersed within the ACC structure.<sup>10</sup> With the organic components present at concentrations typically no more than a few mole % per mole Ca, the bulk composition of gastrolith ACC is similar to that of synthetic, hydrated ACC (nominally  $\text{CaCO}_3 \cdot \text{H}_2\text{O}$ ). It is thus far not well-understood whether the organic components that appear to play a role in the formation and stabilization of the gastrolith ACC<sup>21</sup> also result in an average structure that differs substantially from that of synthetic ACC. The relatively large size of the gastroliths formed in the American lobster (~1 g of gastrolith material from ~600 g lobster) makes them well suited for study by multiple techniques. It has been shown that ACC also occurs in the exoskeleton of the American lobster.<sup>22,23</sup>

## 2. EXPERIMENTAL SECTION

**2.1. Lobster Gastrolith Samples.** Gastroliths were extracted from mature American lobsters in premolt stage. The pair of 1–2 cm discs were rinsed and stored in pure

ethanol (Figure SI-1 of the Supporting Information). To confirm that exposure to ethanol did not modify the structure or the hydrous components of ACC, we tested a series of drying procedures, with and without ethanol, using several types of synthetic ACC. X-ray scattering and NMR results, performed as described in the respective sections below, showed no differences resulting from exposure to ethanol for periods up to 2 weeks.

The gastrolith discs are friable assemblages of horn-shaped pieces that readily disaggregate. SEM imaging of the fracture surface of an individual piece shows it to be composed of spheres ranging in size from 60 to 300 nm (Figure 1). Prior to

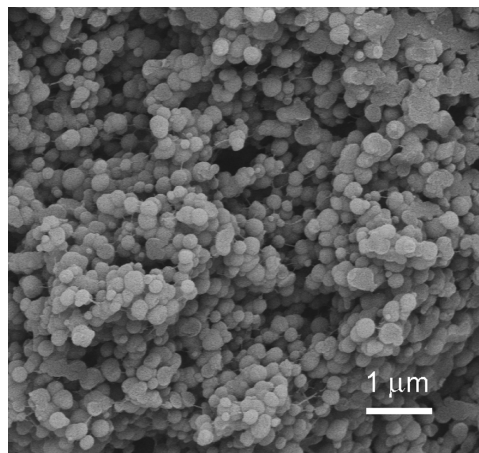


**Figure 1.** SEM image of fracture surface of lobster gastrolith, showing ACC spheres ranging in size from 60 to 300 nm.

characterization, a portion of the gastrolith was gently disaggregated, rinsed, and vacuum-filtered in clean acetone to yield dry sample. Samples were ground lightly in a pestle and mortar prior to analysis. A portion of a sample was dissolved in trace metal-grade  $\text{HNO}_3$  acid for analysis of trace metals by direct-coupled plasma (DCP) spectrophotometry. Only Mg (2870 ppm) and P (9420 ppm) were detected in addition to Ca.

Over the course of the study, dry gastrolith ACC was stored in sealed polybags at ambient conditions over durations up to one year. These aged samples were re-examined to determine if they transform to crystalline calcium carbonate, inasmuch as transformation does not occur within the molt cycle of the lobster.

**2.2. Synthetic ACC Samples.** An additive-free ACC and a  $\text{PO}_4$ -doped ACC were synthesized following the procedure used by Michel et al.<sup>15</sup> and first described by Koga et al.<sup>24</sup> Briefly, calcium chloride and sodium carbonate solutions were rapidly mixed to yield a highly supersaturated solution equimolar in Ca and  $\text{CO}_3$ . Sodium hydroxide was added to maintain a high pH. For the  $\text{PO}_4$ -doped ACC, a sodium phosphate solution was added to give approximately 5 wt %  $\text{PO}_4$ . A white precipitate formed within several seconds and was recovered by vacuum filtration. The solid was rinsed repeatedly with acetone during vacuum filtration to remove water. The solid was then transferred to a lab vacuum for ~30 min to complete drying of the sample. XRD was used to confirm the absence of sharp diffraction peaks as described by Michel et al.<sup>15</sup>

**2.3. Thermogravimetric Analysis and Differential Scanning Calorimetry.** Simultaneous weight loss and heat

flow were measured during programmed heating (30–900 °C at 10 °C/min) using a Netzsch STA449C Jupiter instrument. Approximately 10 mg of dry powdered sample was placed in an alumina crucible and covered with a perforated lid. Dry nitrogen was used as the purge gas.

**2.4. Pair Distribution Function (PDF) Analysis and Extended X-ray Absorption Fine Structure (EXAFS) Analysis.** Total X-ray scattering data for PDF analysis were collected at the sector 11-ID-B beamline ( $\sim 58$  keV,  $\lambda = 0.2127$  Å) at the Advanced Photon Source, Argonne National Laboratory. The PDF is defined as  $G(r) = 4\pi r[\rho(r) - \rho_0]$ , where  $\rho(r)$  is the atomic pair density and  $\rho_0$  is the average atomic number density<sup>25</sup> and was obtained by Fourier transformation of  $F(Q)$  truncated at  $Q_{\max} = 23\text{--}24$  Å<sup>-1</sup>. The composition used in the normalization of each experimental structure function was  $\text{CaCO}_3 \cdot 1.1\text{H}_2\text{O}$ , based on the thermogravimetry results. Further details are given in the Supporting Information.

Calcium K-edge EXAFS data were collected at the sector 20-BM beamline at the Advanced Photon Source (Argonne National Laboratory). ACC or calcite reference material was applied to Kapton tape, and 2–4 layers were used to obtain an edge jump  $0.5 \leq \Delta\mu x \leq 1.5$ . A minimum of four scans were collected for each sample, and scans were averaged after confirming energy calibration. Background subtraction and  $R$ -space fitting were performed using standard methods, which are described in the Supporting Information. On the basis of fits to reference materials, the error in the first-shell distance is  $\pm 0.02$  Å, with errors for more distant shells significantly greater ( $\pm 0.04$  Å). Errors for coordination number (CN) and the Debye–Waller type factors ( $\sigma^2$ ) are estimated as  $\pm 25\%$  and  $\pm 0.002$  Å<sup>2</sup>, respectively.

**2.5. Nuclear Magnetic Resonance (NMR) Spectroscopy.** The <sup>13</sup>C and <sup>1</sup>H NMR spectra were obtained with a 500 MHz (11.7 T) Varian Infinity Plus spectrometer using a probe assembly configured for 5 mm (o.d.) rotors and with a ceramic spinner for reduced background. The sample was removed from storage and quickly loaded into an oven-dried rotor, which was then evacuated at room temperature with a laboratory vacuum for 30 min, repressurized under N<sub>2</sub>, and sealed with press-fit PTFE caps. The <sup>13</sup>C and <sup>1</sup>H chemical shifts are referenced relative to TMS using adamantane as a secondary standard ( $\delta_{\text{C}} = 38.6$  and  $\delta_{\text{H}} = 2.0$  ppm). Crystallization of aged samples was readily detected in <sup>13</sup>C NMR spectra by the appearance of sharp peaks in spectra obtained by direct excitation (DE), greatly reduced intensity in CP/MAS experiments, and appearance of a large narrow peak for liquid water in <sup>1</sup>H DE spectra.

The <sup>31</sup>P{<sup>1</sup>H} CP/MAS NMR spectra were acquired with a 400 MHz (9.4 T) Varian Inova spectrometer, operating at 399.9 and 161.2 MHz for <sup>1</sup>H and <sup>31</sup>P, respectively. The sample was loaded into 3.2 mm (o.d.) thin-walled (36 μL) rotors, using the same procedure as described above and spun at 10 kHz. The <sup>31</sup>P chemical shifts are referenced to 85% H<sub>3</sub>PO<sub>4</sub> using a secondary hydroxylapatite standard set to  $\delta_{\text{p}} = 2.65$  ppm. Further details of NMR data collection procedures are given in the Supporting Information.

### 3. RESULTS

**3.1. Thermal Analysis.** Thermogravimetry shows two main stages of weight loss on programmed heating (10 °C/min). The first stage is complete by  $\sim 250$  °C and involves a weight loss of 15–18% (Figure 2). This corresponds to an endotherm

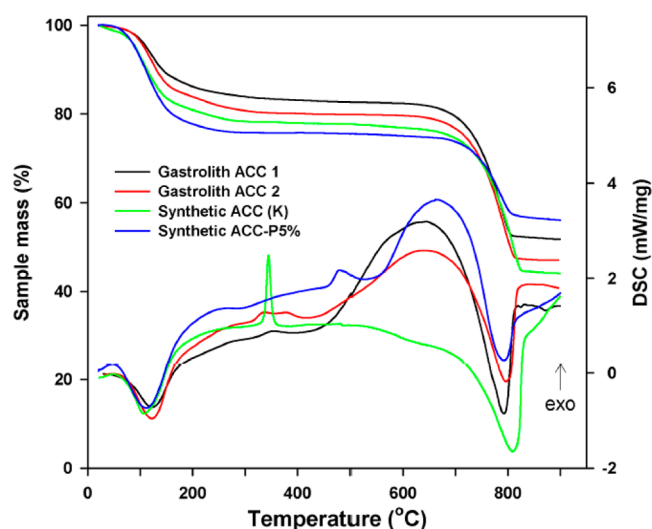


**Figure 2.** Mass loss (top curves; left axis) and heat flow curves (bottom curves; right axis) for two gastrolith ACC samples compared with corresponding curves for an additive-free ACC (K) and a 5 wt % PO<sub>4</sub>-doped ACC.

in the DSC curve and has been attributed to loss of H<sub>2</sub>O.<sup>7,24</sup> The DSC curves for the gastrolith ACC show one or two small exothermic events at 330–370 °C, accompanied by little additional weight loss. XRD reveals that crystallization of calcite occurs within this range. One of these weak features may be attributable to breakdown of chitin, which has been shown to exhibit an exotherm in the range of 290–360 °C.<sup>26</sup> A more significant, broad exotherm is also evident in the temperature range of 500–720 °C, just prior to the second main stage of weight loss beginning at  $\sim 740$  °C and corresponding to the breakdown of calcite to CaO with loss of CO<sub>2</sub>. These TGA and DSC curves show the range of differences observed for gastrolith samples taken from several different lobsters. The weight loss curves are similar to those of the two synthetic ACC samples but with slightly less H<sub>2</sub>O loss in the first stage. The exothermic peak of the additive-free synthetic ACC at 340 °C, corresponding to calcite crystallization, is more distinct than that for the gastrolith ACC. The broad exotherm at higher temperature in the gastroliths is absent in the additive-free ACC, however, a similar exotherm is present in the PO<sub>4</sub>-doped ACC curve. This may suggest that the phosphate component within the gastrolith undergoes a transformation upon heating.

If we assume that the weight loss up to 400 °C, at which temperature ACC has crystallized to calcite, is attributable to loss of H<sub>2</sub>O, the nominal composition of the gastrolith ACC is  $\text{CaCO}_3 \cdot n\text{H}_2\text{O}$ , where  $n = 1.0\text{--}1.2$ . This is consistent with earlier reports for H<sub>2</sub>O content in synthetic, hydrated ACC.<sup>7,15,24,27</sup>

**3.2. Pair Distribution Function Analysis.** The total scattering data for gastrolith ACC were normalized using the approximate composition  $\text{CaCO}_3 \cdot 1.1\text{H}_2\text{O}$ , within the range determined by thermogravimetric analysis. The  $Q_{\max}$  value of  $\sim 23$  Å<sup>-1</sup> was chosen as a compromise between maximizing signal and minimizing the impact of noise inherent at the high scattering vector. The experimental reduced structure function,  $F(Q)$ , and pair distribution function,  $G(r)$ , are shown in Figure 3, along with corresponding experimental functions for a synthetic, hydrated ACC and a calcite reference sample. Total scattering data were collected for several gastrolith samples taken from different lobsters in premolt stage; no differences

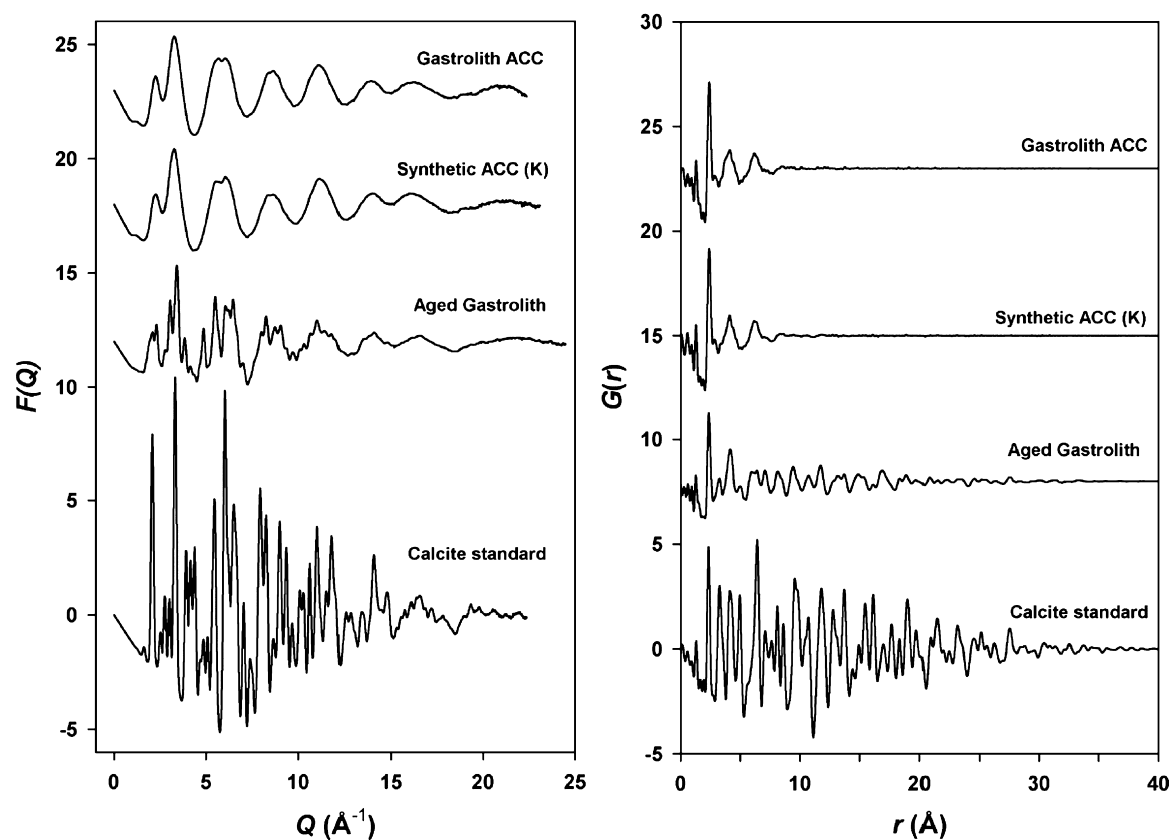


**Figure 3.** X-ray total scattering reduced structure functions,  $F(Q)$ , for ACC, aged gastrolith, and a calcite standard (left). Pair distribution functions,  $G(r)$ , obtained by Fourier transformation of  $F(Q)$  (right).

were found among the data for different samples. The reduced structure function,  $F(Q)$ , for gastrolith ACC shows broad peaks that are characteristic of materials lacking long-range order. The first low- $Q$  peak at  $\sim 2.2 \text{ \AA}^{-1}$  is slightly sharper, as is commonly observed in noncrystalline materials that exhibit medium-range order.<sup>28</sup> Peaks dampen with increasing scattering vector,  $Q$ , as expected, owing mainly to the  $Q$  dependence of atomic scattering factors for X-rays. The  $F(Q)$  function for gastrolith ACC is nearly indistinguishable from that for a synthetic, hydrated ACC, which is comparable to the synthetic samples studied by Michel et al.<sup>15</sup> A very subtle difference is noted between these functions in the small minimum superimposed on the broad peak at  $\sim 6 \text{ \AA}^{-1}$ . Both  $F(Q)$  functions contrast markedly with the function for a calcite standard, in which sharp peaks, characteristic of a crystalline solid, are observed.

The PDFs,  $G(r)$ , were obtained by Fourier transformation of the  $F(Q)$  functions and represent the distribution of interatomic distances.<sup>25</sup> It is noteworthy that H atoms do not contribute to the scattering to any significant degree owing to their very small scattering cross section for X-rays. The PDF for gastrolith ACC exhibits a weak, sharp peak at  $\sim 1.3 \text{ \AA}$  and a strong, sharp peak at  $\sim 2.4 \text{ \AA}$  (Figure 3). A weak peak is also evident at  $\sim 2.9 \text{ \AA}$ , appearing as a small shoulder to the  $2.4 \text{ \AA}$  peak. In addition, there are two broad peaks centered at  $\sim 4$  and  $\sim 6 \text{ \AA}$ , with weak oscillations extending up to  $\sim 10 \text{ \AA}$ . Comparison with the PDF for synthetic ACC shows essentially identical features, in both position and amplitude. Although barely discernible in Figure 3, the PDFs for both ACC samples exhibit high frequency, low-amplitude oscillations as a result of Fourier termination errors, and the convolution of high- $Q$  noise in the  $F(Q)$  functions. These effects are not discernible in the

PDF of the calcite standard. Due to the presence of long-range order in the calcite, peaks in the PDF extend beyond  $40 \text{ \AA}$ , although damping of the peaks with increasing  $r$  occurs as a result of instrumental factors. The absence of peaks at  $r > \sim 10 \text{ \AA}$  in the PDFs for both ACC samples (except for the high-frequency artifacts noted above) confirms that long-range order is not present.

Over the course of the study, the onset of crystallization was observed in dry gastrolith ACC samples as they aged. Figure 3 shows  $F(Q)$  and  $G(r)$  functions for a gastrolith sample aged for 346 d at ambient dry conditions. The  $F(Q)$  function shows sharp peaks emerging, some of which correspond to peaks in the calcite standard. Yet comparison with the  $F(Q)$  functions for ACC reveals that the periodicity of the ACC is still clearly evident. Further analysis of this aged gastrolith shows that it is composed of three phases: ACC, calcite, and vaterite (Figure SI-3 of the Supporting Information). The PDF for the aged gastrolith sample shows peaks extending up to  $30 \text{ \AA}$ , consistent with the development of long-range order during crystallization. More detailed study of the transformation kinetics of gastrolith ACC is deferred for separate reporting.

Because chitin has been reported as a component in crustacean gastrolith, we compared the raw total scattering data from the gastrolith with that for an  $\alpha$ -chitin standard (MP Biomedicals). Chitin produces sharp peaks as expected for a crystalline material. None of the peaks in the chitin standard matched any features in the ACC scattering data (Figure SI-2 of the Supporting Information).

**3.3. X-ray Absorption Spectroscopy.** Calcium K-edge EXAFS spectroscopy has been used extensively to characterize the local structure in ACC.<sup>4,22,27,29,30</sup> The chi function and

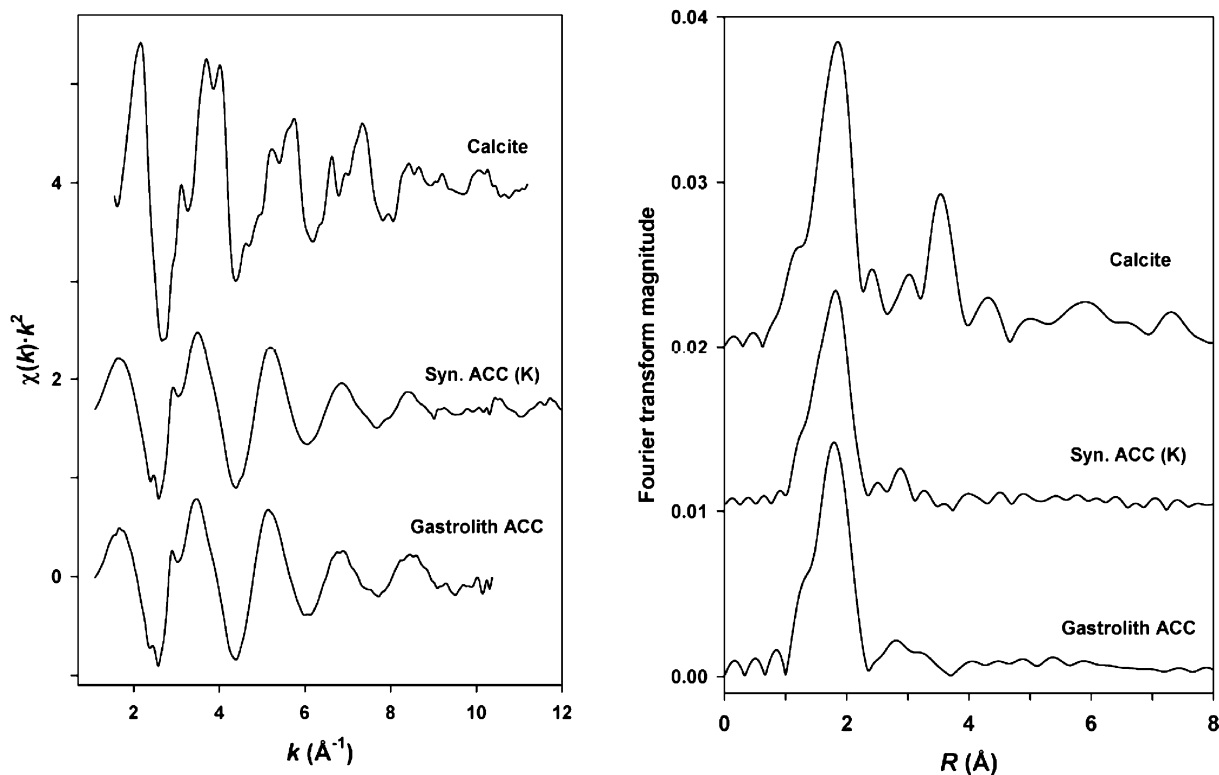


**Figure 4.** Ca K-edge EXAFS chi functions (left) and Fourier transform magnitudes for gastrolith ACC, synthetic ACC, and a calcite standard (right). FT magnitude is not corrected for phase shifts.

corresponding Fourier transform (FT) magnitude for gastrolith ACC are shown in Figure 4. No discernible differences were found among EXAFS data of several samples taken from different lobsters. The chi curve is dominated by a single beat pattern and is found to be nearly identical to that for a synthetic hydrated ACC. Superimposed on this beat are small, sharp features at 2.4, 2.9, and 10.3  $\text{\AA}^{-1}$ , which arise from multielectron excitations.<sup>31</sup> These features are more evident in the chi curves of the amorphous samples because of the decreased amplitude of the backscattering in the disordered phase; they are less evident in the calcite chi curve. The FT magnitude shows a single main peak at low  $R$ . This reflects the first-shell coordination of calcium by oxygen atoms. Weaker features in the FT of the gastrolith ACC are evident at  $\sim 3$   $\text{\AA}$  (not corrected for phase shifts). Similar weak features are found in the FT of the synthetic ACC, and in both cases their positions and amplitudes change as the  $k$  range is varied. The use of a short  $k$  range, partly determined by multielectron excitations, limits the information that can be obtained about potential higher  $R$  shells.

The gastrolith ACC EXAFS was fit in  $R$  space using a single Ca–O shell. This yielded best fit parameters:  $CN = 5.8 (\pm 0.9)$ ,  $R_{\text{Ca-O}} = 2.41 (\pm 0.02)$   $\text{\AA}$ ,  $\sigma^2 = 0.008 (\pm 0.002)$   $\text{\AA}^2$ , and  $E_0 = 0.15$  eV. Fitting of the synthetic ACC gave nearly identical parameters, in agreement with the results of Michel et al.<sup>15</sup>

**3.4. FTIR-ATR.** Previous studies have used FTIR to distinguish ACC from crystalline  $\text{CaCO}_3$ . In particular, attention has been drawn to the strong attenuation of the  $\nu_4$  in-plane bending mode of the  $\text{CO}_3$  group at  $\sim 713$   $\text{cm}^{-1}$  in ACC relative to the  $\nu_2$  out-of-plane bending mode at  $\sim 862$   $\text{cm}^{-1}$  ( $870$   $\text{cm}^{-1}$  in calcite).<sup>1,14</sup> This is evident for the FTIR spectrum for the gastrolith ACC (Figure 5). In comparison to the sharp peak at  $\sim 713$   $\text{cm}^{-1}$  in calcite, this mode is strongly

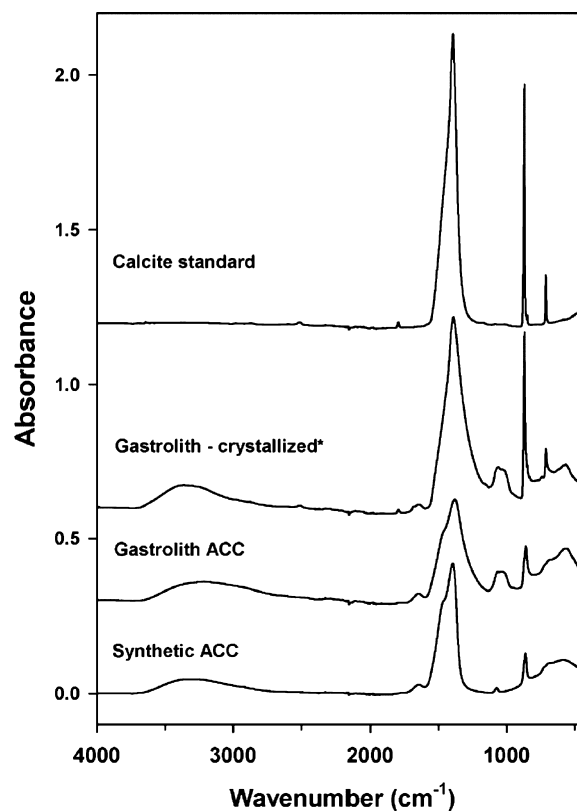


**Figure 5.** FTIR-ATR spectra for gastrolith and synthetic ACC samples and a calcite standard. The spectrum for an aged gastrolith (partially crystallized) is also shown (\*).

attenuated in the gastrolith ACC, and closer inspection reveals that it is actually a weak doublet centered at  $\sim 713\text{ cm}^{-1}$  in both the gastrolith and synthetic ACC spectra. The  $\nu_3$  asymmetric stretching mode at  $1470\text{--}1400\text{ cm}^{-1}$  is split in both the gastrolith and synthetic ACC spectra but is broader overall in the gastrolith spectrum. Other differences are evident between the gastrolith and synthetic ACC spectra. Notably, a weak peak at  $1074\text{ cm}^{-1}$  in the synthetic ACC is obscured by a broad peak centered at  $\sim 1042\text{ cm}^{-1}$  in the gastrolith spectrum, which is attributable to phosphate, known to be present from the bulk analysis. A weak peak is also seen in both ACC spectra at  $\sim 1650\text{ cm}^{-1}$ . Although it has been observed in other FTIR spectra of ACC, its origin in these spectra is unclear. Spectra of phosphates exhibit a peak at this position, as does chitin.<sup>1,19</sup> However, the similarity of this peak in the gastrolith ACC with that in the synthetic ACC spectrum, which is free of both phosphate and chitin, makes it unlikely that either of these minor components is its cause in either spectrum.

Figure 5 also shows the FTIR spectrum of the aged gastrolith in which partial crystallization has occurred. Notable changes in this spectrum, relative to the gastrolith ACC, include a sharp  $\nu_4$  peak at  $\sim 713\text{ cm}^{-1}$ , a narrower  $\nu_3$  asymmetric stretching band at  $1470\text{--}1400\text{ cm}^{-1}$ , and a shift of the broad OH stretching feature at  $3500\text{--}3200\text{ cm}^{-1}$  to higher wavenumber.

**3.5. NMR Spectroscopy.** The gastrolith samples yield  $^{13}\text{C}$  NMR spectra that contain a broad, symmetrical, featureless peak for carbonate groups centered near  $\delta_{\text{C}} = 168.8\text{ ppm}$ ,  $3.6\text{ ppm}$  full-width at half-maximum (fwhm). Within uncertainty, the width and position of the carbonate peak is the same whether acquired by direct excitation (DE) or  $^{13}\text{C}\{^1\text{H}\}$  CP methods (Figure 6) and nearly identical to those reported previously for ACC gastroliths from crayfish.<sup>10</sup> The signal from gastrolith ACC closely resembles that reported previously for synthetic ACC prepared by hydrolysis of dimethylcarbonate and by rapid mixing of  $\text{NaHCO}_3$  and  $\text{CaCl}_2$  solutions ( $\delta_{\text{C}} = 169\text{ ppm}$ ,  $3.6\text{ ppm}$  fwhm)<sup>15</sup> and that synthesized at pH 8.75 in excess ethanol and denoted “pc-ACC” by Gebauer et al. ( $\delta_{\text{C}} = 168.7\text{ ppm}$ ,  $3.5\text{ ppm}$  fwhm).<sup>32</sup> ACC synthesized at pH 9.5 by Gebauer et al. gave a higher chemical shift ( $169.5\text{ ppm}$ ) and crystallized to vaterite rather than calcite.<sup>32</sup> The gastrolith  $^{13}\text{C}$  NMR spectra also contain small peaks for organic molecules centered near 105, 75, 56, and 25 ppm evident in the full spectrum. These peaks account for no more than a few percent of the total intensity and likely arise from the chitin scaffold.<sup>10</sup> Occasionally, aged gastrolith material crystallized in the NMR rotor, which resulted in the appearance of narrow peaks for crystalline vaterite ( $170.6$  and  $169.6\text{ ppm}$ ) and calcite ( $168.7\text{ ppm}$ ) in the DE spectrum (Figure 6, top panel), in agreement with the XRD and PDF results. As found by PDF analysis, a signal from carbonate groups in remnant ACC present in minor amounts can be observed in the CP/MAS spectrum (Figure 6), which is shifted to higher chemical shift ( $169.3\text{ ppm}$ ) and narrower ( $2.9\text{ ppm}$  fwhm) compared to that of the initial gastrolith.

The lobster gastroliths yield a complex DE  $^1\text{H}$  spectrum (Figure 7) containing many overlapping peaks as might be expected for a heterogeneous material of biological origin. The main features include a broad spinning sideband (SSB) envelope spanning  $100\text{ kHz}$  and centered at  $\delta_{\text{H}} = 6.2\text{ ppm}$  (the average of the  $\pm n$  SSB positions), a narrower peak at  $\delta_{\text{H}} = 5.3\text{ ppm}$ , and narrow signals at  $3.8$  and  $1.3\text{ ppm}$  that arise from a small amount of ethanol remaining in the sample. The broad SSB envelope and narrower peak at  $5.3\text{ ppm}$  occur in an

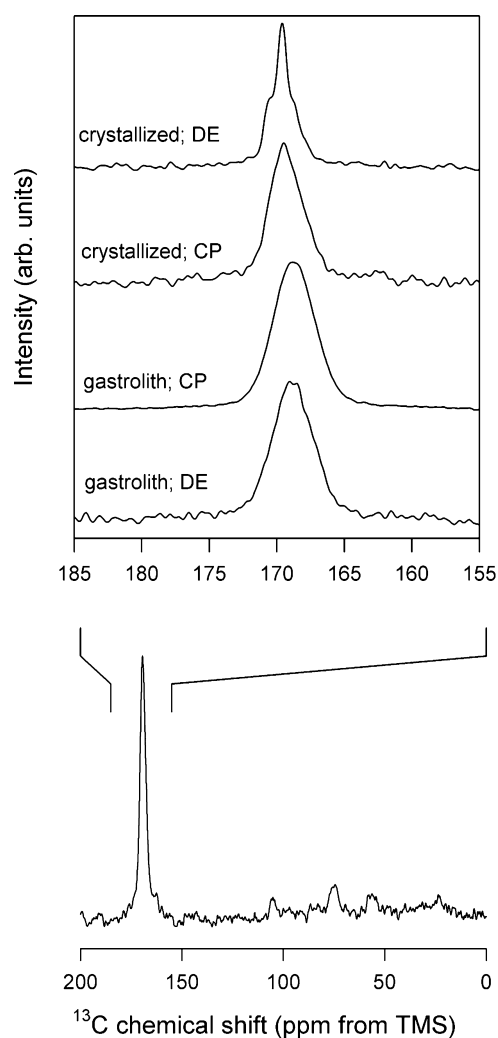


**Figure 6.**  $^{13}\text{C}$  NMR spectra of lobster gastrolith and partially crystallized aged gastrolith obtained by direct excitation (DE) and  $^1\text{H} \rightarrow ^{13}\text{C}$  cross-polarization (CP). Bottom panel shows the full DE spectrum and top panel the expanded chemical shift region for carbonate groups.

approximately 1:1 ratio and closely resemble signals from synthetic ACC assigned to rigid and restrictedly mobile water molecules, respectively.<sup>15</sup> Other signals from the minor concentrations of organic components, including the chitin scaffold, are also likely present but obscured by the abundant water H (H:Ca  $\sim 2$ ). Also shown in Figure 7 is an indirectly detected  $^1\text{H}$  NMR spectrum that was obtained from  $^{13}\text{C}\{^1\text{H}\}$  CP/heteronuclear correlation (hetcor) data by integrating across the ACC  $^{13}\text{C}$  signal. The signal in this spectrum arises from  $^1\text{H}$  that transfer polarization to carbonate carbons during CP and hence are in close proximity to carbonate groups. It contains only a broad spinning sideband envelope, with a center band at a chemical shift near  $+6.3\text{ ppm}$ , within uncertainty the same as that from the DE spectrum. In contrast to previous results for synthetic ACC, there is neither evidence for a narrower signal from more mobile water in the hetcor data nor a peak for hydroxyl groups, which account for about 10% of the H in synthetic, hydrated ACC.<sup>15</sup>

Owing to the high P impurity concentration of the gastrolith ACC noted above,  $^{31}\text{P}$  NMR signal is easily detected by both DE and CP methods (Figure 8). In both cases, a single broad

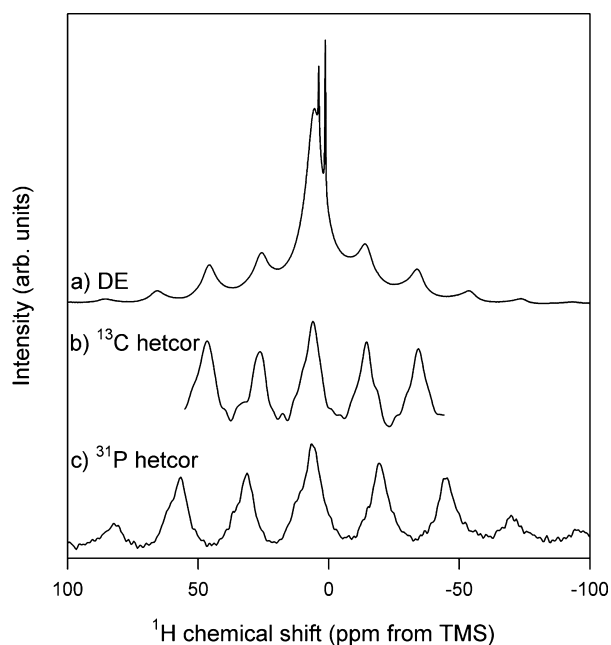


**Figure 7.**  $^1\text{H}$  MAS/NMR spectra of lobster gastrolith, obtained by (a) direct-excitation and indirectly by integrating over the main peak in the F2 dimension of (b)  $^{13}\text{C}\{^1\text{H}\}$  and (c)  $^{31}\text{P}\{^1\text{H}\}$  2-dimensional hetcor spectra.

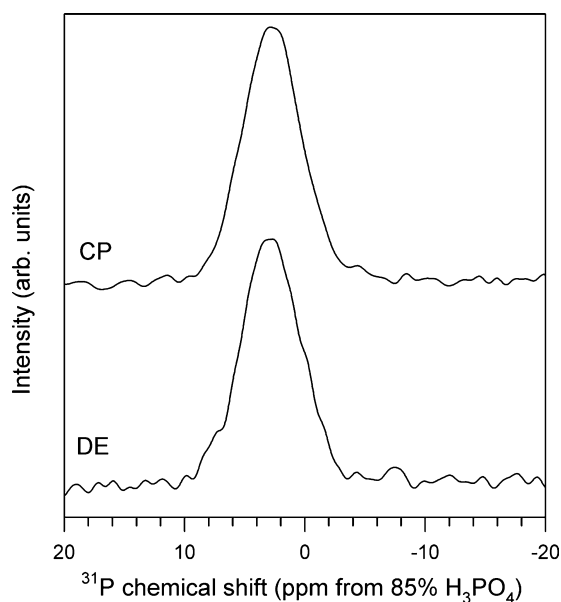


**Figure 8.**  $^{31}\text{P}$  MAS/NMR spectra of lobster gastrolith, obtained by direct excitation (DE) and by  $^{31}\text{P}\{^1\text{H}\}$  CP/MAS (CP).

peak at a chemical shift typical for phosphate groups is observed ( $\delta_{\text{p}} = 2.8$  ppm, 5.7 ppm fwhm). The signal bears some resemblance to that for phosphate defects in crystalline carbonates but occurs at a somewhat lower chemical shift and is broader than observed for phosphate in calcite ( $\delta_{\text{p}} = 3.6$  ppm, 3.7 ppm fwhm)<sup>33</sup> and somewhat narrower than observed for phosphate in aragonite ( $\delta_{\text{p}} = 4$  ppm, 6.4 ppm fwhm).<sup>34</sup> Indirectly detected  $^1\text{H}$  spectra from  $^{31}\text{P}\{^1\text{H}\}$  CP/hetcor contain mainly a broad spinning sideband envelope centered near  $\delta_{\text{H}} = 6.5$  ppm, similar to that obtained via  $^{13}\text{C}$  detection (Figure 7) but with a centerband that is notably asymmetrical toward higher chemical shifts. This asymmetry corresponds to

increased intensity in the +10 to +20 ppm range and can be fit with a peak centered near +15 ppm. This chemical shift is characteristic of acidic or strongly hydrogen-bonded H and is similar to that observed for hydrogen phosphate groups in crystalline Ca phosphates. After aging for several days, a small, narrow cross-peak is clearly evident in 2-dimensional hetcor spectra at chemical shifts characteristic of monetite ( $\delta_{\text{p}} = -1.5$  ppm,  $\delta_{\text{H}} = 13$  ppm; see the Supporting Information).

#### 4. DISCUSSION

Analysis of the X-ray total scattering data and the pair distribution functions shows that the atomic pair correlations observed in the lobster gastrolith ACC appear the same as those observed for synthetic ACC. Both samples are hydrated, with nominal composition,  $\text{CaCO}_3 \cdot \text{H}_2\text{O}$ . As described by Michel et al.,<sup>15</sup> the low- $r$  peaks in the PDF are readily interpreted. The narrow, weak peak at 1.3 Å is due to C–O bonds in  $\text{CO}_3$  groups, which behave as rigid units with little variation in the C–O distance. The strong peak at 2.4 Å is due mainly to Ca–O bonds. This is consistent with the single peak, fit at 2.41 Å, in the Ca K-edge EXAFS, corresponding to the first coordination shell of Ca. In the PDF there is also a lesser contribution to this peak from O–O distances in  $\text{CO}_3$  groups, at  $\sim 2.2$  Å. The intensity of peaks in the PDF reflects the average scattering power of the atom pair as well as the pair correlation probability. Hence Ca–O pairs will contribute more than O–O pairs. It is worth emphasizing again that H atoms do not contribute to any significant degree, owing to their small scattering cross section for X-rays. Therefore, the PDF provides no useful information about O–H bonds, which are clearly evident in the NMR and FTIR spectra.

Among the most significant features of the PDF for the gastrolith ACC are the peaks at  $\sim 4$  and  $\sim 6$  Å, which document the presence of medium-range order, previously identified in synthetic ACC samples only.<sup>15,35</sup> These features are distinctly broader than the peaks at 1.3 and 2.4 Å and correspond to second- and/or third-neighbor distances in the ACC. The greater breadth of these peaks also suggests a range of interatomic distances greater than expected for first-shell coordination. Michel et al. interpreted the broad peaks at  $\sim 4$  and  $\sim 6$  Å as representing Ca–Ca, Ca–O, and (less importantly) Ca–C pair correlations.<sup>15</sup> Goodwin et al. used reverse Monte Carlo (RMC) refinement of the total scattering from synthetic ACC to develop a structure model.<sup>16</sup> Two different linkages between Ca atoms were consistently found throughout their model, with Ca–Ca distances at  $\sim 4$  and at  $\sim 6$  Å. In one linkage, second-neighbor Ca atoms share an oxygen from a  $\text{CO}_3$  group, with an  $\sim 4$  Å separation. In the second case, Ca atoms are linked through two oxygens in the same  $\text{CO}_3$  group, with  $\sim 6$  Å separation. These linkages also occur in crystalline forms of calcium carbonate, but the broad features in the PDF at  $\sim 4$  and  $\sim 6$  Å do not uniquely correspond to any crystalline  $\text{CaCO}_3$  phase, as noted previously.<sup>15</sup>

It is noteworthy that these medium-range correlations involving Ca atoms are not observed in the Ca EXAFS of either the gastrolith or synthetic ACC (Figure 4). This is not surprising, however, inasmuch as the mean free path for photoelectrons is typically no greater than 5–6 Å. Combined with exponential damping of the signal and the limited  $k$  range experimentally attainable at the Ca K edge, the structural information for higher shells (from EXAFS) is severely restricted in ACC phases. In the case of high-energy X-ray total scattering, while damping of the signal still occurs, it is a

less significant factor. Limitations in the instrumental resolution are more important in controlling damping in PDFs. The PDF for calcite (Figure 3) shows the expected decrease in amplitudes for a well-crystallized solid, using the same experimental conditions as for the ACC samples. Distinct correlations extend beyond 30 Å. Moreover, the PDF is not limited to correlations involving a single element (e.g., Ca).

The PDFs for gastrolith and synthetic ACC both show a very weak, broad oscillation centered at  $\sim 9$  Å. Michel et al. also noted very weak oscillations extending to  $\sim 15$  Å in PDFs of synthetic ACC.<sup>15</sup> No correlations are observed in the PDFs for either ACC in this study at  $r$  values greater than  $\sim 10$  Å. As explained earlier, high-frequency, low-amplitude oscillations are evident over this high- $r$  region and represent a combination of Fourier termination errors and the convolution of experimental noise evident in the high- $Q$  range of the reduced structure functions (Figure 3). Nevertheless, the absence of distinct features in the ACC PDFs beyond  $\sim 10$  Å confirms the absence of long-range order.<sup>15</sup> The structural coherence in the gastrolith ACC is several orders of magnitude smaller than the size of the spherical particles observed by SEM. This supports the interpretations of Goodwin et al., who proposed a structure model consisting of a disordered network of multiple Ca coordination environments.<sup>16</sup> Because the PDF for gastrolith ACC is nearly identical to the PDF reported by Michel et al. and used for the RMC modeling by Goodwin et al., the same structure model is expected for the gastrolith ACC, using the same RMC constraints.

Whereas the PDF and EXAFS results from gastrolith ACC revealed few differences with hydrated synthetic samples, our results from NMR spectroscopy suggest notable differences in the short-range structure, relating mainly to the distribution and mobility of H. The principal difference appears to lie in the nature of H associated with carbonate carbon as shown by comparing the  $^1\text{H}$  spectra from  $^{13}\text{C}\{^1\text{H}\}$  CP/hetcor experiments. These data show signal of protons from which polarization is transferred to  $^{13}\text{C}$  nuclei during the CP contact period and other nearby H in mutual dipolar contact. Similar to synthetic ACC, a dominant signal arises from rigid water molecules corresponding to the broad spinning sideband envelope. These rigid waters donate moderately strong hydrogen bonds, as indicated by the  $^1\text{H}$  chemical shift. Unlike synthetic ACC, however, no  $^1\text{H}$  signal from more mobile water can be observed from the gastrolith ACC through  $^{13}\text{C}$  detection, even though such H accounts for approximately one-half the intensity of its directly detected  $^1\text{H}$  spectrum, corresponding to the large peak near +5.5 ppm. This result indicates either that the mobile water is farther away from carbonate groups in the gastrolith ACC or that the motions are isotropic and rapid enough to more effectively remove the dipolar interactions between  $^1\text{H}$  in mobile and rigid water molecules. In addition, synthetic ACC contains a modest fraction of hydroxyl groups, which yield a narrow  $^1\text{H}$  signal near +1.2 ppm and account for approximately 7% of H. No similar signal was observed from the biogenic ACC by either DE or CP/hetcor.

These differences in the distribution of H suggest a likely role in the relative stabilities of synthetic and biogenic ACC. The close proximity of mobile water to carbonate groups in synthetic ACC suggests that this mobility permeates the structure, which could aid transport and rearrangement of carbonate groups necessary to nucleate and grow crystalline phases. The decoupling of mobile water from carbonate groups

in biogenic ACC suggests that the mobile water apparent in the DE  $^1\text{H}$  spectra might occur largely on particle surfaces and in pores or fluid inclusions and thus has much more limited access for promoting rearrangement of carbonate ions. We speculate that the absence of hydroxyl groups in the biogenic ACC may reflect a lower pH in its local environment of formation. The synthetic ACC shown to contain hydroxyl was precipitated at high pH (10.5–11), achieved in part by direct addition of NaOH.

The minor components Mg (2870 ppm) and P (9420 ppm) in the gastrolith ACC do not seem to have any readily discernible influence on the short- or medium-range structure, as indicated by the similarities of the PDFs of the gastrolith and synthetic ACC. The  $^{31}\text{P}$  NMR results suggest that inorganic phosphate is the principal form of P, based on the similarity of the chemical shift to those of Ca orthophosphates<sup>36</sup> and to phosphate defects in calcite and aragonite.<sup>33,34</sup> Organophosphates would be expected to yield peaks at lower chemical shifts if present at sufficiently high concentrations. For example, in addition to a larger peak near +3 ppm for inorganic phosphate, Akiva-Tal et al. observed in  $^{31}\text{P}\{^{13}\text{C}\}$  hetcor spectra of crayfish gastrolith, a broad peak centered near  $\delta_{\text{p}} = -1$  ppm that was attributed to small organophosphate molecules.<sup>10</sup> Similar organophosphate molecules could be present in lobster gastrolith at concentrations too low to be readily apparent (less than about 5% of the total P), considering the broad peak for inorganic phosphate overlaps this chemical shift region. Our observation from NMR spectroscopy that monetite crystallizes as the gastrolith ages suggests that at least some of the phosphate in the lobster gastrolith occurs in an amorphous calcium phosphate (ACP) phase. Such material has been suggested previously to accompany ACC in calcium storage structures (spheruliths) of terrestrial crustaceans based on Raman spectra<sup>7</sup> and in the exoskeletons of crustaceans as inferred from crystallization of apatite upon heating.<sup>37</sup>

Although chitin has been reported as a component of gastroliths in other crustaceans and peaks consistent with its presence in lobster gastrolith were observed by  $^{13}\text{C}$  NMR, we found no evidence for it in either the X-ray total scattering (Figure SI-2 of the Supporting Information) or the FTIR data, possibly owing to a low concentration. Thermal analysis may exhibit permissive evidence for minor chitin. Regardless, the presence of chitin does not appear to have any observable effect on the short- or medium-range structure of gastrolith ACC.

The lobster gastrolith ACC, upon aging under dry ambient conditions, partially crystallizes to form calcite and vaterite (Figure SI-3 of the Supporting Information). In the X-ray PDF this is seen as the appearance of sharp peaks extending beyond 20 Å but clearly lower in amplitude than in the calcite standard (Figure 3). In  $^{13}\text{C}$  NMR spectra distinct, narrow peaks are apparent at positions that match those for these crystalline phases.<sup>15</sup> Yet some ACC is still present in this aged gastrolith after 346 days, as seen by the broad oscillations in the reduced structure function, corresponding with those of the unreacted ACC, and by the broad peak observed by  $^{13}\text{C}\{^1\text{H}\}$  CP/MAS NMR. A distinct shift in the NMR chemical shift of the carbonate carbons from that of the initial ACC suggests that the structure of the ACC evolves as crystallization proceeds. Further characterization of the transformation of gastrolith ACC to crystalline phases is deferred for a more complete study.

## 6. CONCLUSIONS

The combination of techniques we have used here reveals both similarities and differences between biogenic and synthetic, hydrated ACC. The PDF analysis shows that the fundamental structural arrangements of Ca coordination polyhedra are largely similar in the synthetic and biogenic samples studied. This may indicate that precursors to ACC formation (e.g., nanometer-scale clusters) share similarities across a broad range of formation environments. The most pronounced differences between synthetic and biogenic samples involve the hydrous components and are revealed by the  $^1\text{H}$  NMR results. The fewer types of hydrous components in the biogenic sample may suggest a more highly controlled formation environment and/or slower formation kinetics than in the extremely rapid laboratory synthesis. We can speculate that different types and arrangements of the hydrous components can be attributed to subtle differences in aggregation of smaller clusters. If true, then one may expect to see considerable variation in the hydrous components among different ACC samples (synthetic and biogenic), whereas the basic network provided by the arrangements of Ca polyhedra may be largely similar.

Further studies, including other biogenic samples, are needed to determine how these structural differences influence crystallization pathways. This will provide better insight to the structural basis for stability and crystallization behavior of ACC as well as applications in engineered systems.

### ■ ASSOCIATED CONTENT

#### Supporting Information

Details of experimental procedures for PDF, EXAFS, and NMR data collection. Figures showing ACC gastroliths, normalized total X-ray scattering data, and two-dimensional NMR CP/hetcor data. This material is available free of charge via the Internet at <http://pubs.acs.org>.

### ■ AUTHOR INFORMATION

#### Corresponding Author

\*E-mail: [rjreeder@stonybrook.edu](mailto:rjreeder@stonybrook.edu).

#### Present Address

<sup>§</sup>School of Earth and Atmospheric Sciences, Georgia Institute of Technology, Atlanta, Georgia 30332, United States.

#### Notes

The authors declare no competing financial interest.

### ■ ACKNOWLEDGMENTS

This research was supported by the U.S. Department of Energy, Office of Basic Energy Sciences Grant DE-FG02-09ER16017. Total scattering data were collected at sector 11-ID-B, and EXAFS data were collected at sector 20-BM-B, both at the Advanced Photon Source, Argonne National Laboratory. We gratefully acknowledge assistance in data collection from Mahaling Balasubramanian, Kevin Beyer, Karena Chapman, Peter Chupas, and Steve Heald. Use of the Advanced Photon Source was supported by the U.S. Department of Energy, Office of Science, Office of Basic Energy Sciences, under Contract No. DE-AC02-06CH11357.

### ■ REFERENCES

- (1) Addadi, L.; Raz, S.; Weiner, S. *Adv. Mater.* **2003**, *15* (12), 959–970.
- (2) Politi, Y.; Arad, T.; Klein, E.; Weiner, S.; Addadi, L. *Science* **2004**, *306*, 1161–1164.

- (3) (a) Aizenberg, J.; Lambert, G.; Weiner, S.; Addadi, L. *J. Am. Chem. Soc.* **2002**, *124*, 32–39. (b) Aizenberg, J.; Weiner, S.; Addadi, L. *Connect. Tissue Res.* **2003**, *44*, 20–25.
- (4) Becker, A.; Bismayer, U.; Epple, M.; Fabritius, H.; Hasse, B.; Shi, J. M.; Ziegler, A. *Dalton Trans.* **2003**, *4*, 551–555.
- (5) Aizenberg, J.; Lambert, G.; Addadi, L.; Weiner, S. *Adv. Mater.* **1996**, *8*, 222–226.
- (6) (a) Lose, E.; Wilson, R. M.; Seshadri, R.; Meldrum, F. C. *J. Cryst. Growth* **2003**, *254*, 206–218. (b) Raz, S.; Hamilton, P. C.; Wilt, F. H.; Weiner, S.; Addadi, L. *Adv. Funct. Mater.* **2003**, *13*, 480–486.
- (7) Raz, S.; Testeniere, O.; Hecker, A.; Weiner, S.; Luquet, G. *Biol. Bull. (Woods Hole, MA, U.S.)* **2002**, *203*, 269–274.
- (8) Bentov, S.; Weil, S.; Glazer, L.; Sagi, A.; Berman, A. *J. Struct. Biol.* **2010**, *171*, 207–215.
- (9) Politi, Y.; Batchelor, D. R.; Zaslansky, P.; Chmelka, B. F.; Weaver, J. C.; Sagi, I.; Weiner, S.; Addadi, L. *Chem. Mater.* **2010**, *22*, 161–166.
- (10) Akiva-Tal, A.; Kababya, S.; Balazs, Y. S.; Glazer, L.; Berman, A.; Sagi, A.; Schmidt, A. *Proc. Natl. Acad. Sci. U.S.A.* **2011**, *108*, 14763–14768.
- (11) Gong, Y. U. T.; Killian, C. E.; Olson, I. C.; Appathurai, N. P.; Amasino, A. L.; Martin, M. C.; Holt, L. J.; Wilt, F. H.; Gilbert, P. U. P. *A. Proc. Natl. Acad. Sci. U.S.A.* **2012**, *109*, 6088–6093.
- (12) Dujardin, E.; Mann, S. *Adv. Mater.* **2002**, *14*, 775–788.
- (13) Aizenberg, J.; Muller, D. A.; Grazul, J. L.; Hamann, D. R. *Science* **2003**, *299*, 1205–1208.
- (14) Beniash, E.; Aizenberg, J.; Addadi, L.; Weiner, S. *Proc. R. Soc. London, Ser. B* **1997**, *264*, 461–465.
- (15) Michel, F. M.; MacDonald, J.; Feng, J.; Phillips, B. L.; Ehm, L.; Tarabrella, C.; Parise, J. B.; Reeder, R. J. *Chem. Mater.* **2008**, *20*, 4720–4728.
- (16) Goodwin, A. L.; Michel, F. M.; Phillips, B. L.; Keen, D. A.; Dove, M. T.; Reeder, R. J. *Chem. Mater.* **2010**, *22*, 3197–3205.
- (17) (a) Travis, D. F. *Biol. Bull. (Woods Hole, MA, U.S.)* **1960**, *118*, 137–149. (b) Greenaway, P. *1985. Biol. Rev. Cambridge Philos. Soc.* **1985**, *60*, 425–454.
- (18) Luquet, G.; Marin, F. *Comptes Rendus Palevol* **2004**, *3*, 515–534.
- (19) (a) Takagi, Y.; Ishii, K.; Ozaki, N.; Nagasawa, H. *Zool. Sci.* **2000**, *17*, 179–184. (b) Shechter, A.; Berman, A.; Singer, A.; Freiman, A.; Grinstein, M.; Erez, J.; Aflalo, E. D.; Sagi, A. *Biol. Bull. (Woods Hole, MA, U.S.)* **2008**, *214*, 122–134.
- (20) Shechter, A.; Glazer, L.; Cheled, S.; Mor, E.; Weil, S.; Berman, A.; Bentov, S.; Aflalo, E. D.; Khalaila, I.; Sagi, A. *Proc. Natl. Acad. Sci. U.S.A.* **2008**, *105*, 7129–7134.
- (21) Sato, A.; Nagasaka, S.; Furihata, K.; Nagata, S.; Arai, I.; Saruwatari, K.; Kogure, T.; Sakuda, S.; Nagasawa, H. *Nat. Chem. Biol.* **2011**, *7*, 197–199.
- (22) Levi-Kalisman, Y.; Raz, S.; Weiner, S.; Addadi, L.; Sagi, I. *Adv. Funct. Mater.* **2002**, *12* (1), 43–48.
- (23) Al-Sawalmih, A.; Li, C.; Siegel, S.; Fabritius, H.; Yi, S.; Raabe, D.; Fratzl, P.; Paris, O. *Adv. Funct. Mater.* **2008**, *18*, 3307–3314.
- (24) Koga, N.; Nakagoe, Y. Z.; Tanaka, H. *Thermochim. Acta* **1998**, *318*, 239–244.
- (25) Egami, T.; Billinge, S. J. L. *Underneath the Bragg-Peaks: Structural Analysis of Complex Materials*; Plenum: Oxford, 2003.
- (26) Koll, P.; Borchers, G.; Metzger, J. O. *J. Anal. Appl. Pyrolysis* **1991**, *19*, 119–129.
- (27) Levi-Kalisman, Y.; Raz, S.; Weiner, S.; Addadi, L.; Sagi, I. *J. Chem. Soc., Dalton Trans.* **2000**, *21*, 3977–3982.
- (28) Salmon, P. S. *Nat. Mater.* **2002**, *1*, 87–88.
- (29) Politi, Y.; Levi-Kalisman, Y.; Raz, S.; Wilt, F.; Addadi, L.; Weiner, S.; Sagi, I. *Adv. Funct. Mater.* **2006**, *16*, 1289–1298.
- (30) Gunther, C.; Becker, A.; Wolf, G.; Epple, M. *Z. Anorg. Allg. Chem.* **2005**, *631*, 2830–2835.
- (31) Fulton, J. L.; Heald, S. M.; Badyal, Y. S.; Simonson, J. M. *J. Phys. Chem. A* **2003**, *107* (23), 4688–4696.
- (32) Gebauer, D.; Gunawidjaja, P. N.; Ko, J. Y. P.; Bacsik, Z.; Aziz, B.; Liu, L.; Hu, Y.; Bergstrom, L.; Tai, C.-W.; Sham, T.-K.; Eden, M.; Hedin, N. *Angew. Chem., Int. Ed.* **2010**, *49*, 8889–8891.

- (33) Mason, H. E.; Frisia, S.; Tang, Y.; Reeder, R. J.; Phillips, B. L. *Earth Planet. Sci. Lett.* **2007**, *254*, 313–322.
- (34) Mason, H. E.; Montagna, P.; Kubista, L.; Taviani, M.; McCulloch, M.; Phillips, B. L. *Geochim. Cosmochim. Acta* **2011**, *75*, 7446–7457.
- (35) Radha, A. V.; Fernandez-Martinez, A.; Huc, Y.; Jun, Y.-S.; Waychunas, G. A.; Navrotsky, A. *Geochim. Cosmochim. Acta* **2012**, *90*, 83–95.
- (36) Belton, P. S.; Harris, R. K.; Wilkes, P. J. *J. Phys. Chem. Solids* **1988**, *49*, 21–27.
- (37) Becker, A.; Ziegler, A.; Epple, M. *Dalton Trans.* **2005**, 1814–1820.